J Mater Sci: Mater Electron (2016) 27:4526–4533
DOI 10.1007/s10854-016-4327-6

Effects of superconducting parameters of SnO_2 nanoparticles addition on (Bi, Pb)-2223 phase

Şeyda Yavuz[1] · Özlem Bilgili[1] · Kemal Kocabaş[1]

Received: 10 September 2015 / Accepted: 10 January 2016 / Published online: 2 February 2016

Abstract In this work, nano-SnO_2 (<100 nm) added samples in $Bi_{1.7-x}Pb_{0.3}Sn_xSr_2Ca_2Cu_3O_y$ (x = 0.00–0.20) were prepared by conventional solid-state reaction method. The phase formation, volume fraction and lattice parameters were characterized using X-ray powder diffraction measurements. Surface morphology and grain connectivity of the samples were identified by using scanning electron microscope (SEM). Diamagnetic onset temperatures (T_c^{on}) and hole concentration (p) of SnO_2 added samples were determined by ac susceptibiliy measurements. AC susceptibility measurements showed that diamagnetic onset temperatures (T_c^{on}) of samples Sn0 (x = 0.00), Sn1 (x = 0.05), Sn2 (x = 0.10), Sn3 (x = 0.15) and Sn4 (x = 0.20) are 108.559, 109.985, 101.281, 101.670 and 92.676 K, respectively. SEM measurements showed that not only the surface morphology and grain connectivity degrade but also the grain size of the samples decrease with the increase of the Sn addition. Also, addition of SnO_2 nanoparticles increases the impurities, voids and porosity. X-ray diffraction patterns of all samples indicated the majority of Bi-2223 and Bi-2212 phases along with minor impurity phase Ca_2PbO_4. The volume fraction of the Bi-2223 phase for the sample with x = 0.10 SnO_2 showed the highest percentage (49.49) and with further increasing SnO_2, the volume fraction of the Bi-2223 phase decreases and Bi-2212 phase increases. All SnO_2 nanoparticles added samples showed quite similar lattice parameters compared with non-added sample. These results indicate that nano SnO_2 does not have significant impact on the lattice parameters.

1 Introduction

Since 1980s, the investigation of high temperature superconductor materials has taken great attention. The discovery of Bi-based high temperature superconductor ceramics has helped to improve the most promising materials which can be used for technological and industrial applications [1]. In order to enhance superconducting, electrical, magnetic and mechanical properties of these materials, different dopants have been made [2, 3]. The BSCCO families are known as $Bi_2Sr_2Ca_{n-1}Cu_nO_{2n+4+\delta}$, where n = 1, 2 and 3. (Bi, Pb)-2201, (Bi, Pb)-2212 and (Bi, Pb)-2223 phases are characterized by high superconducting transition temperatures 20, 95 and 110 K, respectively [4].

Chemical doping and introduction of nano-sized particles in bulk high-T_c superconductors have generated great interest because they serve as an easily controlled and efficient tool for improving the superconducting properties [5]. Recently, addition of nano-particles to (Bi, Pb)-2223 phase has been effective in enhancing the flux pinning, critical current density and critical temperature. It has been reported that the addition of ZrO_2 [6], SiC [7], MgO [8], Al_2O_3 [9, 10], Cr_2O_3 [11] in Bi-2223 improves the flux pinning of this system [4, 12]. However, this addition could produce defects within superconducting grains [9].

Nanotechnology developments enabled synthesize of a wide range of nanostructure materials. In the nanosize range, the particles have high proportion of atoms located at their surface compared to bulk materials, increasing unique physical and chemical properties that are very different from their bulk counterparts. In recent years, the

✉ Özlem Bilgili
ozlem.bilgili@deu.edu.tr

[1] Department of Physics, Dokuz Eylul University, 35160 Buca Izmir, Turkey

studies on the effect of addition or substitution of nanoparticles in BSCCO system has become area of interest. When nanoparticles are added to the BSCCO system, they settle easier and much more among the grains of these ceramic superconductors than the micro size dopants due to the tiny size of nanoparticles. If adequate amount of nanoparticles with metallic character is added to the BSCCO, the intergrain connectivity will possibly improve. Nanostructured materials are with structural features in between those of atoms/molecules and bulk materials, with at least one dimension in the range of 1–100 nm [13–17]. Coherence length is $\xi = 2.9$ nm and penetration depth is $\lambda = 60$–1000 nm for $Bi_2Sr_2Ca_2Cu_3O_{10}$ system. Thus, nanoparticle addition between 2.9 and 60 nm in which superconducting properties may be improved have been studied in various works [18, 19].

The influence of SnO_2 nanoparticles addition on (Bi, Pb)-2223 superconducting phase formation and superconducting properties have been studied in various works. Abou-Aly et al. [4] has reported the influence of SnO_2 nanoparticles addition with different concentrations to the phase formation, microstructure, electrical and thermal properties of (Bi, Pb)-2223 phase. In their study, the volume fraction, the superconducting transition temperature and critical current density had optimal values at x = 0.4 wt%. Garnier et al. [3] observed the influence of the addition of SnO_2 nano-particles on Bi-2223 phase formation as well. It was found that c parameter of Bi-2223 phase increases with SnO_2 addition. Awad et al. [20] investigated the influence of SnO_2 nano-particles addition on Vickers Microhardness of (Bi, Pb)-2223 superconducting phase. The results showed that SnO_2 nanoparticles addition had a significant effect on improving the microhardness of the phase. The microhardness of Bi-2223 phase increases with SnO_2 nano-particles addition up to x = 0.4 wt%. Agail et al. [21] reported the effect of nanosize SnO_2 addition on (Bi, Pb)-Sr–Ca–Cu–O superconductor. This work showed that critical current density and transition temperature have optimal values at x = 0.02 wt%. Bushra et al. [22] studied the improvement of superconducting properties of (Bi, Pb)-2223 added with nano-particles SnO_2. The results indicated that SnO_2 nano particle enhanced the (Bi, Pb)-2223 phase formation by increasing volume fraction of high T_c phase up to x = 0.4 wt %.

In this work, the effects of nano SnO_2 (average size <100 nm) addition on the microstructure and superconducting properties of $Bi_{1.7-x}Pb_{0.3}Sn_xSr_2Ca_2Cu_3O_y$ was studied. Superconducting samples of $Bi_{1.7-x}Pb_{0.3}Sn_xSr_2Ca_2Cu_3O_y$ with different SnO_2 nanoparticles concentrations ($0.00 \leq x \leq 0.20$) were prepared using solid-state reaction method. Structural and magnetic characterizations of the samples were performed by X-ray powder diffraction (XRD), scanning electron microscopy (SEM) and ac susceptibility measurements.

2 Experimental details

Superconducting samples with chemical composition $Bi_{1.7-x}Pb_{0.3}Sn_xSr_2Ca_2Cu_3O_y$ (x = 0.00, 0.05, 0.10, 0.15, 0.20) were prepared using a conventional solid-state reaction method. The starting materials were Bi_2O_3, PbO, $SrCO_3$, $CaCO_3$, CuO and SnO_2 with average size <100 nm (from Aldrich) (purity ≥ 99.99 %). Stoichiometric amounts of these powders were weighted by Scaltec balance. After weighting, they were thoroughly mixed and ground using an agate mortar and pestle. They were calcined in air at 800 and 820 °C for 20 h with intermediate grinding. The obtained product after calcinations was ground once more. Then, these powders were pressed under 450 MPa pressure using a press machine to form them into pellets of 13 mm diameter and 2 mm thickness. The prepared pellets were sintered at 845 °C for 120 h in air. Samples were cooled in furnace up to room temperature after each cycle. The samples were labelled as Sn0 (x = 0.00), Sn1(x = 0.05), Sn2 (x = 0.10), Sn3 (x = 0.15) and Sn4 (x = 0.20).

Morphological and structural analyses of the samples were performed by SEM and XRD, respectively. The magnetic properties were measured by the mutual inductance method. The prepared samples were characterized using X-ray diffraction (XRD) with CuK_α radiation (CuK_α radiation, $\lambda = 0.154$ nm) in the range $2\theta = 3°$–60°. The density of the samples were calculated with the Archimedes method. AC susceptibility measurements of the samples were performed using a home-made susceptometer and a lock-in amplifier (MODEL SR830 DSP Lock-in Amplifier). The temperature variation was enhanced using a closed cycle helium cryostat equipped with a temperature controller. AC field amplitudes of 20, 40, 80 and 160 A/m were used and frequency was fixed at 1000 Hz. Susceptibility data taken from lock-in amplifier were recorded by using Labview computer software.

3 Results and discussion

Figure 1 shows X-ray diffraction patterns of samples Sn0, Sn1, Sn2, Sn3 and Sn4. Characteristic peaks corresponding to different phases were labelled with different sembols which are filled circle, open circle, filled four pointed star and indicate the peaks due to the Bi-2223 phase, Bi-2212 phase, and Ca_2PbO_4, respectively. The position of the peaks and intensities of diffraction data reveal that all samples consisted of a mixture of Bi-2223 and Bi-2212

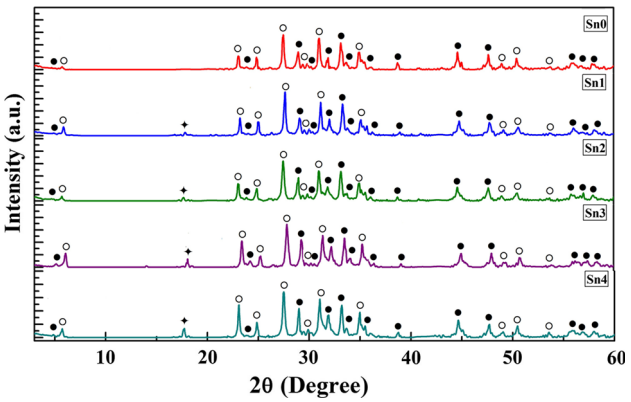

Fig. 1 XRD patterns of the $Bi_{1.7-x}Pb_{0.3}Sn_xSr_2Ca_2Cu_3O_y$ (x = 0.00, 0.05, 0.10, 0.15, 0.20) samples; *filled circle* Bi-2223 phase, *open circle* Bi-2212 phase, *filled four pointed star* Ca_2PbO_4

phases as the major constituents and non-superconducting phase Ca_2PbO_4 as the minor. The first peak H002, at $2\theta \sim 4.7°$, corresponds to (Bi, Pb)-2223 phase whereas the second peak L002, at $2\theta \sim 5.7°$, corresponds to (Bi, Pb)-2212 phase. The first peak intensity decreases while the second peak intensity increases with nano SnO_2 addition up to x = 0.20. A characteristic impurity phase Ca_2PbO_4 peak is at $2\theta \sim 17.8°$. According to XRD results, addition of SnO_2 nanoparticles has increased the intensity of Ca_2PbO_4.

In this study, all peaks of Bi-2223 and Bi-2212 phases have been used for the estimation of the volume fraction of the phases. The volume fractions of the Bi-2223 and Bi-2212 phases were calculated from all peak intensities of Bi-2223 and Bi-2212, using the following equations;

$$\mathrm{Bi}-(2223)\% = \frac{\sum \mathrm{I}(2223)}{\sum \mathrm{I}(2223)+\mathrm{I}(2212)} \times 100$$

$$\mathrm{Bi}-(2212)\% = \frac{\sum \mathrm{I}(2212)}{\sum \mathrm{I}(2223)+\mathrm{I}(2212)} \times 100$$

where I is the intensity of the Bi-2223 and Bi-2212 phases [23–26]. The volume fraction of the phases for all the sample is given in Table 1. As seen in the table, the volume fraction of Bi-2223 phase decreases from 48.18 to 47.60 for the samples having x = 0.00–0.05 and increases to 49.49 for x = 0.10 and then decreases from 49.49 to 44.74 for the samples having x = 0.10–0.20. The sample with x = 0.10 has shown the highest volume fraction of Bi-2223 phase among the others. The intensity of the peaks corresponding to the Bi-2223 phase decreases and the intensity of peaks corresponding to the Bi-2212 phase increases with further increase of SnO_2. The lattice parameters (a, b, c) are calculated from Miller indices (hkl) and interplanar distances (d_{hkl}) by least squares method for all prepared samples. The lattice parameters (a, b, c) of the samples is given in Table 2. The lattice parameters of Bi-2223 and Bi-2212 for the pure sample are a = b = 0.407 Å and c = 37.250 Å and a = 5.4065 Å, b = 5.4051 Å and c = 30.737 Å, respectively. Almost, the same lattice parameters were obtained for the Sn nanoparticles-added samples. The results indicate that SnO_2 nanoparticles added samples showed almost no change in the lattice parameters. This can be explained as a result of the fact that nano-SnO_2 does not enter the (Bi, Pb)-2223 crystal structure, meaning SnO_2 acts only at the grains boundaries.

Table 1 Volume fractions of Bi-2223, Bi-2212 phases and grain size for samples Sn0, Sn1, Sn2, Sn3 and Sn4

Sample	Volume fraction (%)		Grain size (nm)
	Bi-2223	Bi-2212	
Sn0	48.18	51.82	32
Sn1	47.60	52.40	28
Sn2	49.49	50.51	34
Sn3	47.36	52.64	31
Sn4	44.74	55.26	32

The crystallite size was estimated from the broadening of XRD peaks, using Scherrer's formula. The advantage of Scherrer's formula is that the nanometric order of crystallite sizes can be estimated. The values of grain size of samples were calculated by using Scherrer Formula. Scherrer's Equation;

$$L = \frac{0.9\lambda}{t\cos\theta}$$

In equation, L is the crystalline size in nm, λ is the wavelength of X-ray in nm, t is the FWHM of the highest intensity peak and θ is corresponding angle of the peak [27]. The results of the crystallite size are shown in Table 1. The grain sizes calculated from XRD patterns lies between 28 and 34 nm.

The density of samples were measured according to the Archimedes principle in pure water and air. Density was calculated by using the equation;

$$\rho = \frac{\mathrm{W(h)}[\rho(\mathrm{s})-\rho(\mathrm{h})]}{0.99813[\mathrm{W(s)}-\mathrm{W(h)}]} + \rho(\mathrm{h})$$

where ρ(h) and ρ(s) are in air and pure water densities and W(h) and W(s) are their weights. The density of samples were shown in Table 3. The densities are 5.2006, 5.3438, 5.3056, 5.2802 and 5.2324 g/cm^3 for samples Sn0, Sn1, Sn2, Sn3 and Sn4, respectively. Sn1 has the highest density value. The theoretical density of BPSCCO system is found as 6.3 g/cm^3 from the lattice parameters [28–30]. The density of pellets are calculated by geometrical measurements and found to be in the range of 3.8–4.1 g/cm^3. The bulk densities determined by the Archimedes method are in the 82.5–85 % range of theoretical density. The bulk

Table 2 Lattice parameters (a, b, c) for samples Sn0, Sn1, Sn2, Sn3 and Sn4

Sample	Lattice parameters (Bi-2223 phase)			Lattice parameters (Bi-2212 phase)		
	a (Å)	b (Å)	c (Å)	a (Å)	b (Å)	c (Å)
Sn0	5.407	5.407	37.250	5.406	5.405	30.737
Sn1	5.406	5.408	37.203	5.405	5.394	30.688
Sn2	5.405	5.410	37.156	5.406	5.405	30.737
Sn3	5.406	5.408	37.203	5.406	5.405	30.737
Sn4	5.407	5.407	37.250	5.406	5.405	30.737

Table 3 Density for the samples Sn0, Sn1, Sn2, Sn3 and Sn4 versus doping ratio

Sample	Density (g/cm^3)
Sn0	5.2006
Sn1	5.3438
Sn2	5.3056
Sn3	5.2802
Sn4	5.2324

densities of the samples are also determined from their mass and geometrical dimensions to obtain the information about the structure (porosity) of the samples. These pellets have 34.5–40 % porosity. The variation of the density of samples with SnO_2 nano-particles concentrations is shown in Fig. 2.

AC susceptibility measurement is used for the characterization of inter-grain and intra-grain features of the high temperature superconductor ceramics. The temperature dependencies of the real part $\chi'(T)$ and imaginary part $\chi''(T)$ of ac susceptibility for all samples under the different ac magnetic field values of 20, 40, 80, 160 A/m with f = 1000 Hz is shown in Fig. 3a–e. The real component of ac susceptibility $\chi'(T)$ shows two significant drops when the temperature is decreased below onset of diamagnetic transition for superconductor samples. The first sharp drop is due to the transition within grains and the second drop is due to the occurrence of the superconducting coupling between grains. As seen from Table 4, the diamagnetic onset temperatures (T_c^{on}) of the superconducting transition are 108.559, 109.985, 101.281, 101.670 and 92.676 K for the samples Sn0, Sn1, Sn2, Sn3 and Sn4, respectively. The maximum value of T_c^{on} is observed in the sample with x = 0.05. The variation of T_c with SnO_2 nano-particles for $Bi_{1.7-x}Pb_{0.3}Sn_xSr_2Ca_2Cu_3O_y$ (x = 0.00–0.20) is shown in Fig. 4. The superconducting transition temperature shifted to lower temperatures with increasing Sn addition.

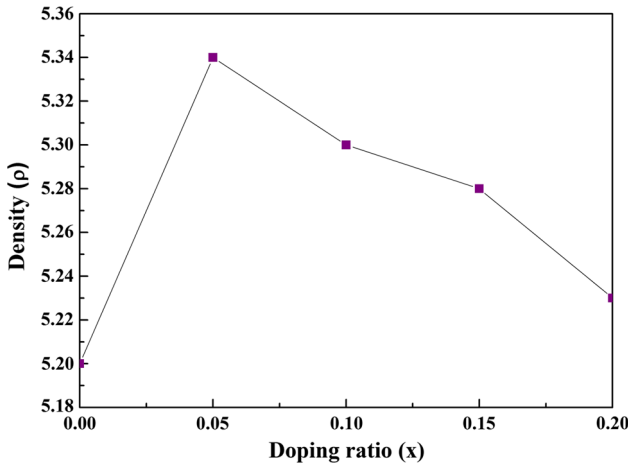

Fig. 2 Density of the samples versus doping ratio

In particular, the imaginary component, $\chi''(T)$, of the ac magnetic susceptibility has been widely used to probe the nature of weak links in polycrystalline superconductors. The imaginary part, $\chi''(T)$, shows a peak, which is a measure of dissipation in the sample. When the peak of $\chi''(T)$, shifts to lower temperatures and broadens, the intergranular coupling between the grains, the critical current density and the flux pinning energy decrease. It can clearly be seen from Fig. 3a–e that the imaginary part of ac susceptibility $\chi''(T)$ depends on the applied ac field. The temperature where maximum peak is observed in the imaginary part (T_p) has decreased with increasing applied field to the sample. As the field amplitude increases, the peak of χ'' shifts to lower temperatures. The amount of the shift as a function of the field amplitude is proportional to the magnitude or strength of the pinning force [31]. The loss peak temperature (T_p) shows the temperature where applied external magnetic field reaches center of the sample and the intensity of this peak is proportional to the energy loss within the intergrain area during the diamagnetic transition. AC loss peak temperature (T_p) represents the full flux penetration in the out of phase component of the samples. As seen from Table 4, the loss peak temperatures (T_p) are 62–59, 60–59, 58–55, 63–60 and 55–52 K for the samples Sn0, Sn1, Sn2, Sn3 and Sn4, at 160–20 A/m ac field, respectively. With increasing the field amplitude H_{ac}, the χ'' signal shifts to lower temperatures. This result demonstrates that the intergranular coupling decreases with increasing ac field amplitude [32].

The variation of peak temperature T_p versus the ac magnetic field for all samples is given in Fig. 5. Müller critical state model accepts a magnetic flux independent pinning force density, α_J and a for intergranular vortices described by the relation:

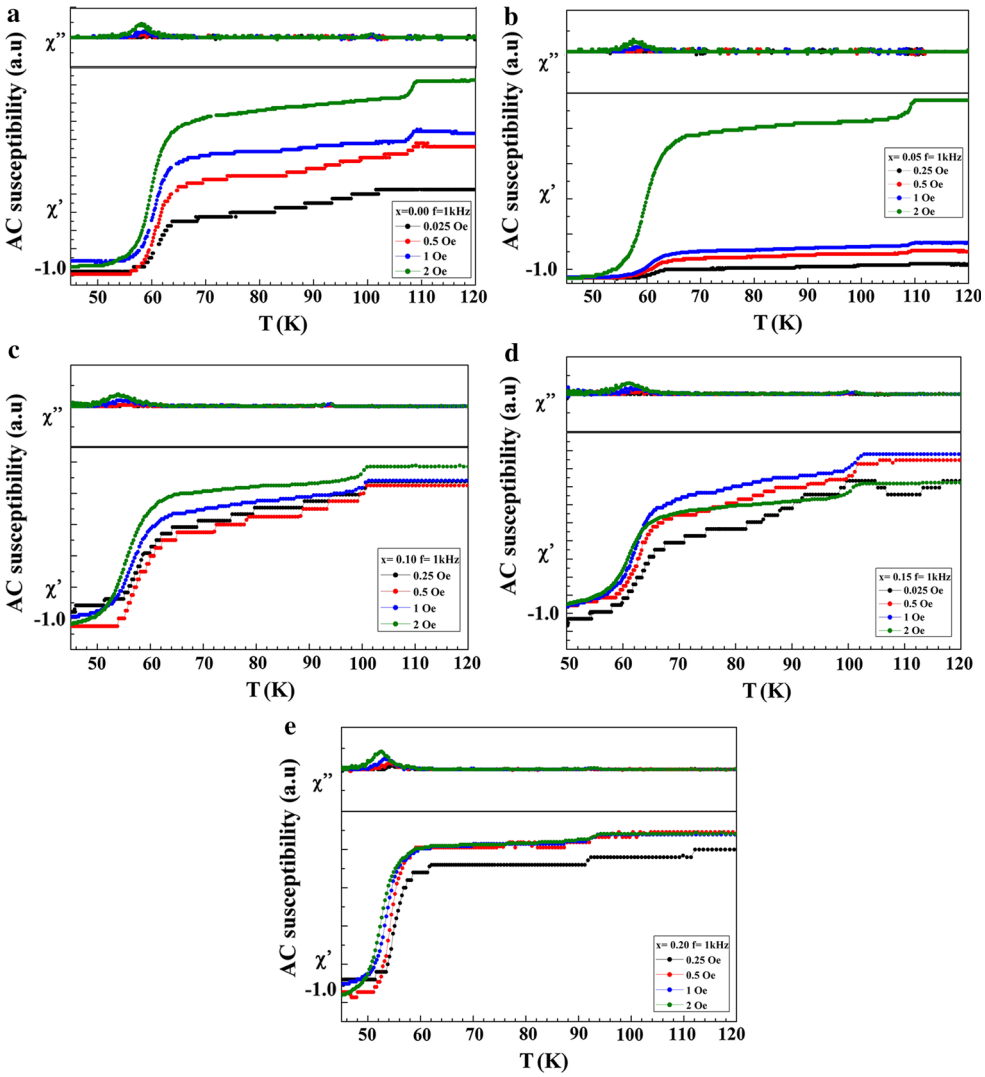

Fig. 3 Real and imaginary parts of ac susceptibility versus temperature for **a** Sn0, **b** Sn1, **c** Sn2, **d** Sn3 and **e** Sn4 in various ac field amplitudes at a frequency of 1 kHz

Table 4 T_c^{on} and T_p temperature of Sn0, Sn1, Sn2, Sn3 and Sn4 samples at different field amplitudes

Sample	T_c^{on} (K)	T_p (K)			
		20 (A/m)	40 (A/m)	80 (A/m)	160 (A/m)
Sn0	108.559	62.136	61.364	60.886	59.948
Sn1	109.985	60.261	58.220	60.408	59.157
Sn2	101.281	58.626	56.013	55.535	55.223
Sn3	101.670	63.864	63.239	61.404	60.954
Sn4	92.676	55.223	53.972	53.494	52.557

$$T_p = T_{p0} - T_{p0}U^{1/2}H_{ac}$$

where U is

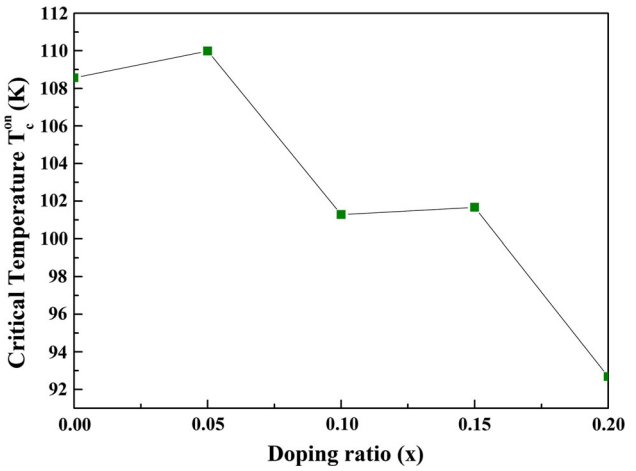

Fig. 4 Variation of T_c versus SnO_2 content for $Bi_{1.7-x}Pb_{0.3}Sn_xSr_2Ca_2Cu_3O_y$ (x = 0.00, 0.05, 0.10, 0.15, 0.20)

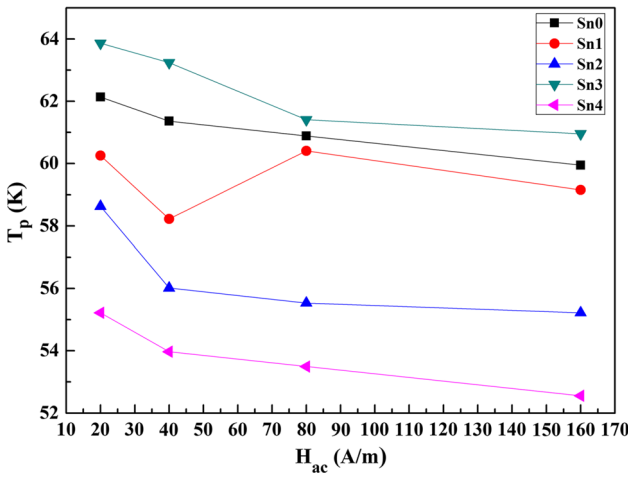

Fig. 5 Intergranular peak temperature versus ac magnetic field amplitude for Sn0, Sn1, Sn2, Sn3 and Sn4 samples

$$U = \frac{\mu_0 \mu_{eff}}{2a\alpha_J(0)}$$

In equation, $\mu_{eff}(0)$ is the effective permeability of the ceramic, a is the length of the samples, and $\alpha_J(0)$ is the intergranular pinning force density [33, 34]. The slope of each line is proportional to $(\alpha_J(0))^{-1/2}$ and the vertical intercept of each line corresponds to the peak temperature, T_{p0}, at zero ac magnetic field amplitude. The values of U are calculated from the slope of each line and shown in Table 5. The decreasing trend in U indicates that the values of intergranular pinning force density $\alpha_J(0)$ increase due to the inverse ratio between U and $\alpha_J(0)$. Hence the sample with x = 0.05 has the highest intergranular pinning force density.

All cuprate families allow non-stoichiometry indicating that carrier hole concentration can be changed continuously by various methods without changing crystall structure. The hole concentrations of superconducting cuprates can be varried by substitution of metallic atoms, by adding excess oxygen atoms or reducing oxygen atoms. In conventional superconductors, the critical temperature increases monotonically with growth of charge carriers, $T_c(p) \propto p$. In cuprates, this dependence is non-monotonic. In most of hole-doped cuprates, the $T_c(p)$ dependence has the bell-like shape. Superconductivity occurs within the limits, $0.05 \leq p \leq 0.27$, which vary slightly in various cuprates [35].

Table 5 The values of U for the pure and SnO_2 added samples

Sample	U $(\alpha_J(0)^{-1/2})$
Sn0	0.01437
Sn1	0.00188
Sn2	0.01854
Sn3	0.02068
Sn4	0.01665

It is well understood that for an optimum hole concentration the T_c has a maximum value and above and below this optimum, T_c decreases. The decrease in the hole concentration might be responsible for degradation of superconducting properties. A parabolic relationship holds between the superconducting transition temperature and the hole concentration p. The hole concentration p is calculated by using the formula:

$$p = 0.16 - \left[\left(1 - T_c/T_c^{max}\right)/82.6\right]^{1/2}$$

where, T_c^{max} is taken as 110 K for (Bi, Pb)-2223 system [36]. It was observed that hole carrier concentration decreases from 0.160 to 0.115 with increasing SnO_2 addition and decreasing T_c, as shown in Fig. 6. The sample with x = 0.05 has the highest value of hole carrier concentration which is 0.160.

Grain structure is one of the most important properties of high transition temperature ceramic superconductors. These grain structures can be examined by SEM photographs. Surface morphology micrographs for all samples are shown in Fig. 7a–e. As SnO_2 nano-particles addition increases, the grain size reduces, the impuruties, porosity and voids increase indicating addition of SnO_2 nanoparticles acts as a barier and hinder the grain growth. In the samples, all of the grains leaded randomly and grain boundaries seem to be in touch with each other soas to make weak bonds which is one of the most important properties of high transition temperature in ceramic superconductors. We believe that white particles sited between the grains are SnO_2 nanoparticles, which is obvious in the micrographs of SnO_2 added samples. Increases of the porosity with more random distribution of

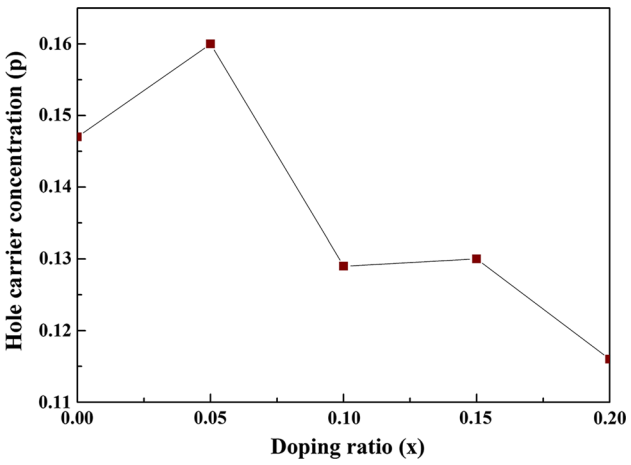

Fig. 6 The variation of hole carrier concentrations versus SnO_2 content for $Bi_{1.7-x}Pb_{0.3}Sn_xSr_2Ca_2Cu_3O_y$ (x = 0.00, 0.05, 0.10, 0.15, 0.20)

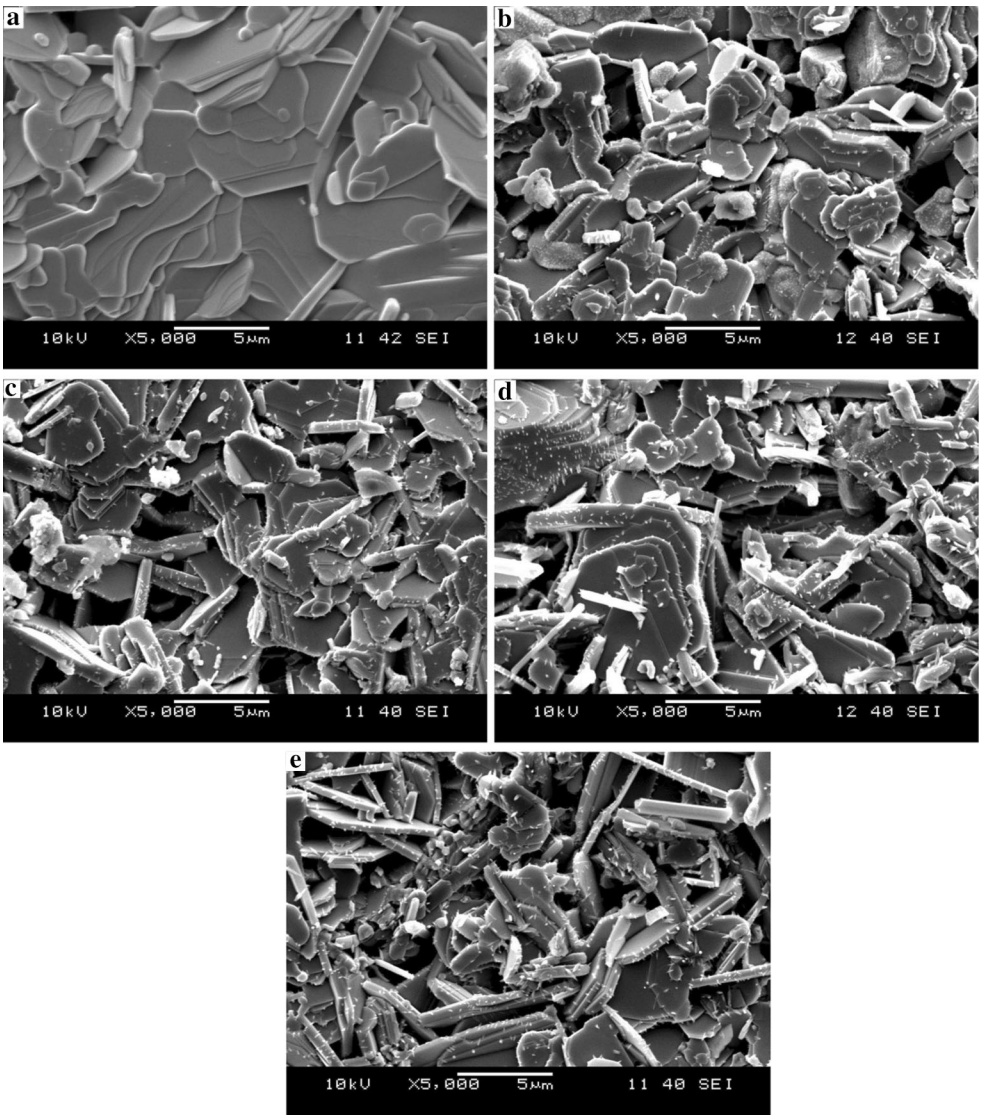

Fig. 7 SEM micrographs of **a** Sn0, **b** Sn1, **c** Sn2, **d** Sn3 and **e** Sn4 samples

grains are seen at samples with SnO_2 nanoparticles added samples compared to undoped sample, which may cause to a decrease in superconducting properties of this sample.

4 Conclusions

In this work, we studied the effects of SnO_2 nanoparticles addition on the phase formation, microstructure and critical temperature of (Bi, Pb)-2223 superconducting phase using XRD, SEM and ac susceptibility measurements. Superconducting samples with chemical composition $Bi_{1.7-x}Pb_{0.3}Sn_xSr_2Ca_2Cu_3O_y$ ($x = 0.00$, 0.05, 0.10, 0.15 and 0.20) were prepared by the conventional solid-state reaction method.

XRD indicated that both Bi-2223 and Bi-2212 phases coexisted in the samples. Volume fraction of Bi-2223 phase increases up to 49.49 with increasing SnO_2 nanoparticles concentration up to $x = 0.10$ and decreases to 44.74 with $x = 0.20$, while the lattice parameters (a, b, c) were almost not affected. It was also found that Bi-2212 phase on the grain boundaries is likely to play the role of weak links and hence reduces the intergranular coupling. The surface morphology and grain connectivity of samples were analyzed by using SEM. It was observed that the microstructures of all samples exhibit a common feature of plate-like grains and are randomly distributed. As addition of nano-Sn increases, the size of plate-like grains slightly decreases, whereas voids and porosity increase. SEM photographs showed that SnO_2 nano-particles addition degraded the grain connectivity. With increasing SnO_2, the grains started to degrade by random orientation, showing weak links between them. This increases the level of impurities, voids and porosity associated with the

formation of smaller plate-like grains which belong to (Bi, Pb)-2212 phase. These results are consistent with that of XRD, which showed a decrease in the volume fraction of the Bi-2223 phase and an increase of Bi-2212 phase. The magnetic characterizations and critical temperature values of the samples were revealed by ac susceptibility measurements. The sample with $x = 0.05$ addition showed the highest superconducting transition temperature, T_c ($\sim$110 K). The hole carrier concentration of sample with $x = 0.05$ was found to be greater than the others. AC susceptibilty measurements showed that the intergranular coupling between the grains, the critical current density and the flux pinning energy of the samples decreased by increasing the amount of SnO_2. It was observed that SnO_2 nanoparticle (<100 nm) had a degradation effect on superconductivity of the Bi-based materials. The higher concentrations of SnO_2 nanoparticles $x > 0.05$ reduced phase formation and superconducting transition temperature of (Bi, Pb)-2223 superconducting phase. This may be attributed to the high concentration of SnO_2 nanoparticles, induced large agglomerations between superconducting grains and hence reduced superconducting grain connectivity. From our study results, it can be stated that addition of SnO_2 nano-particles had a significant role in deteriorating of superconducting properties which is different than previous studies.

References

1. B. Özçelik, M. Gürsul, A. Sotelo, M.A. Madre, J. Mater. Sci. Mater. Electron. **26**, 441–447 (2015)
2. J. Taghipour, H. Abbasi, H. Sedghi, Phys. B. **405**, 1349–1352 (2010)
3. V. Garnier, S. Marinel, G. Desgardin, J. Mater. Sci. **37**, 1785–1788 (2002)
4. A.I. Abou-Aly, M.M.H. Abdel Gawad, R. Awad, J. Supercond. Nov. Magn. **24**, 2077–2084 (2011)
5. A. Ghattas, M. Annabi, M. Zouaoui, F. Ben Azzouz, M. Ben Salem, Phys. C. **468**, 31–38 (2008)
6. Z.Y. Jia, H. Tang, Z.Q. Yang, Y.T. Xing, Y.Z. Wang, G.W. Qiao, Phys. C **337**, 130–132 (2000)
7. Y.C. Guo, Y. Tanaka, T. Kuroda, S.X. Duo, Z.Q. Yang, Phys. C. **311**, 65–74 (1999)
8. W. Wei, J. Schwartz, K.C. Goretta, U. Balachandran, A. Bhargava, Phys. C. **298**, 279–288 (1998)
9. M. Annabi, A.M. Chirgui, F.B. Azzouz, M. Zouaoui, M.B. Salem, Phys. C. **405**, 25–33 (2004)
10. A. Ghattas, M. Annabi, M. Zouaoui, F.B. Azzouz, M.B. Salem, Phys. C. **468**, 31–38 (2008)
11. K. Wei, R. Abd-Shukor, J. Electr. Mater. **36**, 1648–1651 (2007)
12. H. Baqiah, S.A. Halim, M.I. Adam, S.K. Chen, S.S.H. Ravandi, M.A.M. Faisal, M.M. Kamarulzaman, M. Hanif, Solid State Sci. Technol. **17**, 81–88 (2009)
13. A. Zelati, A. Amirabadizadeh, A. Kompany, H. Salamati, J. Sonier, J. Supercond. Nov. Magn. **27**, 2185–2193 (2014)
14. A. Nabil, A. Yahya, R. Abd-Shukor, J. Supercond. Nov. Magn. **27**, 329–335 (2013)
15. A. Agail, R. Abd-Shukor, Appl. Phys. A. **112**, 501–506 (2013)
16. W. Kong, R. Abd-Shukor, J. Supercond. Nov. Magn. **23**, 257–263 (2010)
17. R. Mawassi, S. Marhaba, M. Roumié, R. Awad, M. Korek, I. Hassan, J. Supercond. Nov. Magn. **27**, 1131–1142 (2013)
18. U.Al Khawaja, M. Benkraouda, I.M. Obaidat, S. Alneaimi, Phys. C. **442**, 1–8 (2006)
19. M. Hafiz, R. Abd-Shukor, Appl. Phys. A. **120**, 1573–1578 (2015)
20. R. Awad, A.I. Abou-Aly, M.M.H. Abdel Gawad, I. G-Eldeen, J. Supercond. Nov. Magn. **25**, 739–745 (2012)
21. A. Agail, R. Abd-Shukor, Solid State Sci. Technol. **22**, 1–6 (2014)
22. A. Bushra, A. Aljurani, M.N. Aldulaimi, Int. J. Curr. Eng. Technol. **5**, 1205–1210 (2015)
23. K. Kocabas, O. Bilgili, N. Yasar, J. Supercond. Nov. Magn. **22**, 643–650 (2009)
24. M. Romié, S. Marhaba, R. Awad, M. Kork, I. Haasan, R. Mawassi, J. Supercond. Nov. Magn. **27**, 143–153 (2014)
25. O. Bilgili, K. Kocabas, J. Mater. Sci. Mater. Electron. **25**, 2889–2897 (2014)
26. S. Safran, A. Kılıc, E. Kılıcarslan, H. Ozturk, M. Alp, E. Asikuzun, O. Ozturk, J. Mater. Sci. Mater. Electron. **26**, 2622–2628 (2015)
27. M. Anis-ur-Rehman, J. Alloys Compd. **469**, 66–72 (2009)
28. K. Kocabas, O. Özkan, O. Bilgili, Y. Kadıoglu, H. Yılmaz, J. Supercond. Nov. Magn. **23**, 1485–1492 (2010)
29. K. Kocabas, M. Ciftcioglu, Phys. Stat. Sol. **177**, 539 (2000)
30. X. Yang, T.K. Chaki, Supercond. Sci. Technol. **6**, 343 (1993)
31. S. Çelebi, Phys. C **316**, 251–256 (1999)
32. D. Marconi, G. Stiufiuc, A.V. Pop, J. Phys **153**, 012022 (2009)
33. K.H. Müler, S.J. Collocott, R. Driver, Phys. C. **191**, 339 (1992)
34. O. Ozturk, M. Akdogan, C. Terzioglu, A. Gencer, J. Phys. **153**, 012024 (2009)
35. O. Bilgili, K. Kocabas, J. Mater. Sci. Mater. Electron. **26**, 1700–1708 (2015)
36. O. Bilgili, Y. Selamet, K. Kocabas, J. Supercond. Nov. Magn. **21**, 439–449 (2008)